Understanding Tribology and Machining Processes through Computationally Intensive Large Scale MD

P. A. Romero, M. Moseler

published in

NIC Symposium 2016
K. Binder, M. Müller, M. Kremer, A. Schnurpfeil (Editors)

Forschungszentrum Jülich GmbH,
John von Neumann Institute for Computing (NIC),
Schriften des Forschungszentrums Jülich, NIC Series, Vol. 48,
ISBN 978-3-95806-109-5, pp. 199.
http://hdl.handle.net/2128/9842

Understanding Tribology and Machining Processes through Computationally Intensive Large Scale MD

Pedro A. Romero[1,2] **and Michael Moseler**[1,3,4]

[1] Fraunhofer Institute for Mechanics of Materials IWM,
Wöhlerstraße 11, 79108 Freiburg, Germany
E-mail: michael.moseler@iwm.fraunhofer.de

[2] Karlsruhe Institute of Technology, IAM-CMS, Kaiserstraße 12, 76131 Karlsruhe, Germany

[3] University of Freiburg, Physics Department,
Hermann-Herder-Straße 3, 79104 Freiburg, Germany

[4] Freiburg Materials Research Center, Stefan-Meier-Straße 21, 79104 Freiburg, Germany

We show in two examples how massive molecular dynamics simulations can provide a more fundamental understanding of tribology and machining processes of nanocrystalline metal surfaces. First, we show how a rigid indenter sliding over a nanocrystalline metal surface can cause surface folding during unconstrained plastic surface flow. In this case, the evolution of surface plastic flow and the subsequent folding of the initial surface are dictated by the initial orientation of the surface grains along with the lattice defects extending to the free surface. The folded surface grows into a rough chip with stratified lamellae that are identified as the precursors of wear debris.

The behaviour is very different when the counter surfaces are of similar hardness. Tribological shearing of polycrystalline metals typically leads to grain refinement at the sliding interface. Here, however, we show that nanocrystalline metals exhibit qualitatively different behaviour. Specifically, large time and space scale atomistic simulations demonstrate, that during sliding, contact interface nanocrystalline grains self-organise through extensive grain coarsening and lattice rotation until the optimal plastic slip orientation is established. Afterwards, plastic deformation is frequently confined to localised shear bands aligned with the shearing direction and emanating from voids and other defects in the vicinity of the sliding interface. These findings demonstrate the importance of surface texture and grain structure engineering to achieve ultralow wear in metals.

1 Introduction

The fundamental atomistic mechanisms responsible for friction and wear on polycrystalline metal surfaces are not accessible with conventional experimental setups and/or typical continuum level modelling frameworks like finite elements (FE) modelling or computational fluid dynamics (CFD). In order to establish a fundamental understanding of shear and wear mechanisms on metal surfaces during machining processes, large scale computationally intensive atomistic simulations of polycrystalline metal substrates are necessary. Such simulations require efficient parallel molecular dynamics (MD) algorithms[1] that can run on high performance computers[2]. Typically, metal surfaces under tribological loads are in contact only at certain asperity peaks where most of the initial surface deformation takes place[3,4]. The size of these asperity contacts can be of the order of tens or hundreds of nanometres, which is accessible to large scale classical MD. Therefore the mechanisms responsible for local plasticity and grain structure evolution as well as the different processes

mitigating the sliding motion can to a large extent be studied using large scale classical MD simulations. In tribology and machining processes involving surfaces with different hardness, understanding the unconstrained plastic flow (UPF) of polycrystalline metallic surfaces in sliding contact with hard asperities is crucial for the control of wear in metal-based tribological systems[3–5] and the generation of surfaces in metal-working processes[6–8]. The wear resistance of metallic machine parts can be influenced by preconditioning – either by the final manufacturing steps[9,10] (such as lapping, honing, and grinding) or by suitable running-in procedures during the initial life of a tribological contact[11]. Traditionally, models of UPF have been based on smooth laminar material displacement[5] – an assumption whose general validity has recently been challenged by experimental *in situ* observations and FE simulations of the disruption of laminar flow via folding on a microcrystalline copper surface sliding against a hard steel wedge[12]. Unfortunately, FE lacks the description of the atomistic and crystallographic details underlying the deformation mechanisms responsible for the folding process. Consequently, the microscopic origins of UPF-induced folds in polycrystalline metallic surfaces are still not well understood.

In a tribological process involving surfaces with similar hardness, it is unclear how the initial grain structure at the shear interface will evolve and how the evolving grain structure will accommodate the shear deformation. There exists clear experimental evidence of grain refinement during sliding of conventional polycrystalline metals[13–15]. In contrast, grain growth has been observed in various nanocrystalline metals (Cu[16], Al[17], Ni[18], Ni-Fe and Ni-W[19]). Therefore, it is still unclear whether nanocrystalline metals undergo grain refinement or coarsening. And even though tribo-induced coarsening might be expected, due to the tendency of contacting surfaces to develop highly deformable layers at the contact interface[20,21] and the lower ductility of nanocrystalline metals relative to their microcrystalline counterparts, the exact mechanisms governing this grain growth are hardly understood.

In this communication, we use massive (millions of atoms) atomistic simulations to shed light on the basic mechanisms underlying fold formation during UPF between a hard asperity and a nanocrystalline metal surface. We demonstrate in detail that bulges in front of a moving indenter with a -45^o rake angle are dictated by grains with slip systems that are favourably oriented with respect to the indenters cutting plane. For two nanocrystalline metal surfaces with similar hardness, large-scale atomistic simulations reveal local grain coarsening at the sliding interface followed by significant twinning and the formation of localised nano-shear bands (NSB).

2 Methods

2.1 Hard Asperity on Metal Sliding

The plowing of a nanocrystalline (nc) copper surface by a rigid tapered indenter (asperity) is studied by massively parallel MD[1] employing an embedded atom method (EAM) potential[25]. The surface is modelled as a 160x40x30 nm^3 block (see Fig. 1). To construct the copper surface, a Voronoi algorithm is used to create a fully periodic system with 1584 randomly oriented grains (see top-right of Fig. 1) with grain diameters ranging from 4 to 12 nm. The constructed substrate contains $\sim$15.41 million atoms. The initial Voronoi construction is first optimised with the fast inertial relaxation engine (FIRE)[26] before annealing

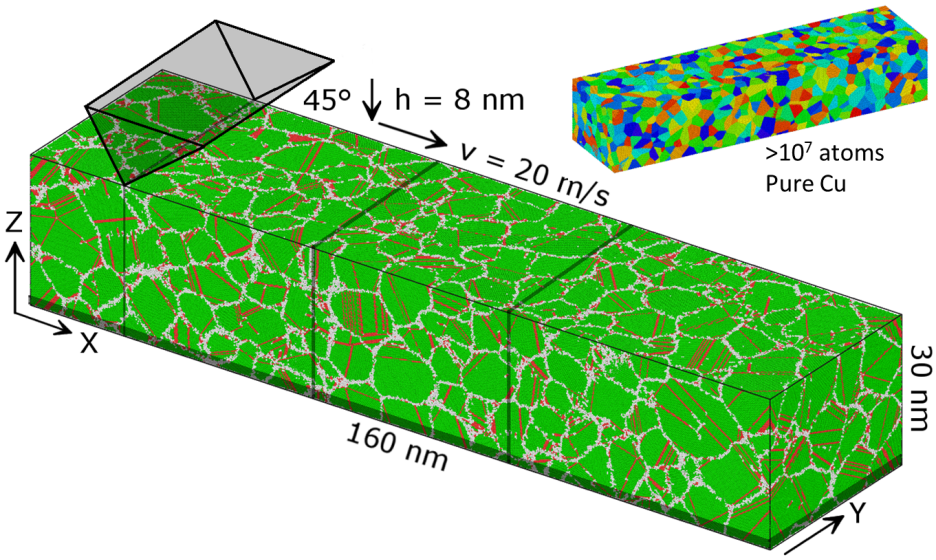

Figure 1. Molecular dynamics simulation of unconstrained surface plastic flow. (a) Copper nanocrystalline substrate and rigid indenter model. Atoms are coloured according to their local environment using a common neighbour analysis (CNA)[20]. Green spheres represent atoms with an fcc environment; red spheres indicate stacking fault and twin boundary atoms; and gray spheres locate GBs and other defect sites. The grains are randomly oriented and contain defects characteristic of annealed copper[21–24].

the sample by heating and holding it at 80% of the melting temperature (T_m = 1152 K) for 500 ps followed by cooling it to 300 K within 50 ps and finally holding the sample at 300 K for 50 ps in order to create a system with relaxed grains and grain boundaries. The temperature changes are conducted within 10 ps respectively with a Berendsen thermostat[27] while holding the pressure constant at 0 GPa with a Berendsen barostat. During annealing, the system dimensions shrink to 158.8x39.5x29.6 nm^3. After annealing, the system acquired an approximate log normal distribution of grains ranging in size from 4 to 18 nm.

During the plowing simulations, periodic boundary conditions are employed in the lateral directions and a 0.5 nm layer of fixed atoms at the bottom of the block mimics the anchoring of the Cu nano-film to a large sample. The indenter is modelled as a nonreactive rigid wedge [with a 90^o opening angle; see Fig. 1] interacting with the Cu surface via a harmonically repulsive potential with a stiffness of 32 Nm^{-1} per atom and a 0.5 nm cutoff. A 300 K dissipative particle dynamics (DPD) thermostat[29] with a dissipation constant of 0.1 eV ps $Å^{-2}$ and a cutoff of 0.45 nm is applied to all atoms in the system in order to reflect ambient temperature and to reduce thermally induced grain growth[21,28] in nc-Cu.

2.2 Metal on Metal Sliding

For sliding contact between metal surfaces with similar hardness, we employed interatomic potentials based on the embedded atom method[30,25] that provide a reliable and efficient description of the atomic interactions for the investigated metals within the temperature

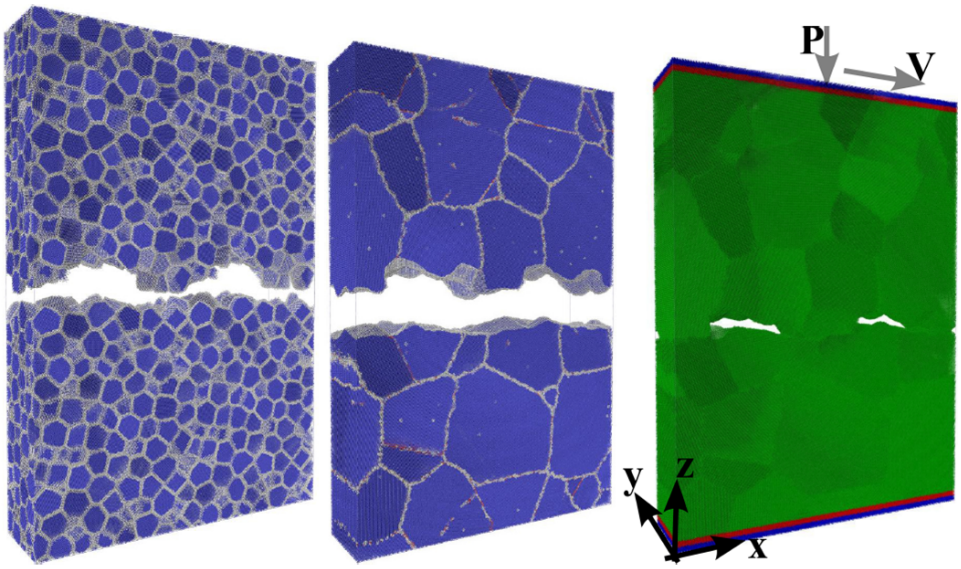

(a) Voronoi construction (b) Annealed Grain Struture (c) Tribomodel: Onset of sliding

Figure 2. (a) Initial Voronoi construction. (b) Final annealed relaxed nanocrystalline counter bodies where blue/grey/red stand for bcc/nonbcc/twin iron atoms base on CNA analysis[20]. (c) Depiction of the tribosystem at the onset of sliding where green/red/blue represent Newtonian/thermostated/rigid atoms.

range of our loading conditions[31]. Here, we present the results for a system consisting of nanocrystalline iron counter surfaces, which corresponds to a controlled volume around a pair of interacting asperities between mated nanocrystalline metal surfaces. To construct this system a Voronoi algorithm was used to generate pure nanocrystalline fully periodic iron counter bodies with randomly oriented grains having an average grain size of $\sim$5 nm. Next, a region with approximately two semi-circles is cut out of the initial Voronoi construction in order to roughen the contacting surfaces (see Fig. 2(a)). The generated system has dimensions of 59.4x14.9x89.1 nm^3 and contains $\sim$5.6 million atoms. In order to prepare the system, the initial construction is annealed by first heating the sample to $\sim 0.85 T_m$ or 1500 K (for iron) for the employed interatomic potential and holding the system at this temperature for $\sim$2.0 ns. Subsequently, the system is quenched to 300 K within a time of $\sim$1.0 ns and then held at 300 K for an additional $\sim$1.0 ns in order to ensure and verify that the annealed grains and grain boundaries are fully relaxed and stable at 300 K (see Fig. 2(b)). After applying and equilibrating a 1 GPa pressure, the system is sheared at a velocity (V) of 5 m/s for $\sim$58 ns under average constant pressure ($\sim$1 GPa) by slightly damping (0.451 (Ev/Å)/(Å/ps)) the vertical motion of the top rigid zone[32].

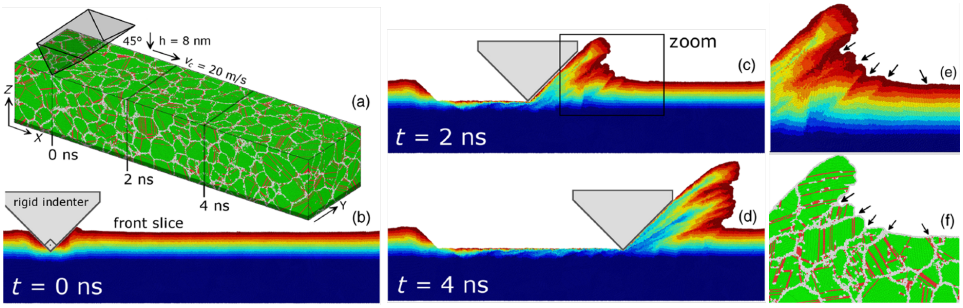

Figure 3. Molecular dynamics simulation of unconstrained surface plastic flow. (a) CNA view of Cu nanocrystalline substrate and indenter. (b)(d) Sequence of snapshots [at the times and indenter positions indicated in (a)] showing an xz cross section of the Cu substrate. In (b)-(d) the atoms have been coloured according to their initial vertical position revealing the initiation and evolution of folding patterns during plowing. (e) Close-up of the chip shown in (c). (f) Same as (e) but coloured according to CNA.

3 Results and Discussion

3.1 Hard Asperity on Metal Sliding

In order to generate UPF on a metal nanocrystalline (nc) surface with a rigid asperity (see Fig. 3(a)), the surface is first indented to a depth of h = 8 nm with a velocity of v_i = 20 m/s. This already results in significant material pileup (see cross-sectional view in Fig. 3(b) where atoms have been coloured according to their initial vertical position). Subsequently, the nc copper is plowed at constant height (h) and a velocity of v_c = 20 m/s. The buildup of pronounced fold patterns is clearly observed during the evolution of UPF. Fig. 3(c) shows a snapshot of the system at t = 2 ns. The folding leads to the formation of a chip with a rough front face [Fig. 3(d)]. Similarities to the micron-scale folds of Ref. 12 are apparent.

The mechanisms governing the formation of surface folds can be understood by inspecting the microstructure of the copper film[34]. A close-up of the chip in Fig. 3(c) (marked by a black frame) is shown in Fig. 3(e) along with additional arrows that mark the notches between the surface protrusions. The observed notches occur consistently at lattice defects (i.e. grain boundaries (GB)) as exhibited by the common neighbour analysis in Fig. 3(f) for the same atoms in Fig. 3(e). Clearly, the arrows coincide with gray zones in Fig. 3(f) representing GBs that separate crystalline areas (green zones).

Fig. 3(e) also shows that the grains at the surface bulge outwards towards the free surface to different degrees. The geometric form of the indenter with a -4^o rake angle suggests that an optimal crystal orientation for outward flow contains a slip system whose slip direction coincides with the rake face and motion of the indenter. In order to quantify the ability of a grain to support a certain shear deformation, an atomic stress projection factor (ASPF) is defined as follows. First, for each atom with an fcc environment the projections $m_s = \cos\varphi_s \cdot \cos\lambda_s$ are calculated for the $s = 1, \ldots 12$ fcc slip systems. Here, λ_s are the angles between the normal of the indenter's rake face and the normals of the $\{111\}$ slip planes of the atomic fcc environment. φ_s denote the angles between chip flow direction (reflecting the upwards material transport along the -45° rake angle) and the $\langle 110 \rangle$ slip directions of the atomic fcc environment of the grain. For each grain, the ASPF

is defined as the maximum m_s of the 12 fcc slip systems similar to the Schmid factor for uniaxial deformation. Indeed, surface grains with higher ASPF tend to exhibit higher degrees of bulging towards the surface[34].

At some arrows in Fig. 3(e), discontinuities in the strata of the initial-z colour scheme can be discerned at GBs which may indicate GB sliding[35] as one mechanism that plays a role in the initiation of bulging and fold formation in nc metals. As shown in Fig. 3(f), the generated chip consists of coarsened larger grains, which form and merge from the start of the plowing. The underlying mechanisms are lattice reorientation and grain boundary migration. Both processes, bulging and coarsening, are evidently linked with the motion of dislocations and their interaction with the GBs. While dislocation-assisted GB migration may generally occur in deforming materials[36] and contribute to the deformation of polycrystalline materials by shear coupling[37], it can also contribute by clearing the path for plastic slip towards the surface in favourably oriented grains and by straightening the GBs parallel to suitably oriented slip planes.

3.2 Metal on Metal Sliding

For surfaces with similar hardness, the interaction between the counter metals is very different relative to hard asperities sliding on metal surfaces. The key stages of deformation for metal on metal sliding contact are presented in Fig. 4. Initially, the relative motion is primarily accommodated via surface grain boundary sliding between the grains forming the initial contact interface [see the bottom panel in Fig. 4(a)]. Accordingly, the starting grain structure is not significantly altered during the initial 4 ns of sliding.

The corresponding evolution of the encountered shear resistance τ(t) and of the ratio of non-bcc to bcc atoms R(t) are presented in Fig. 5(a). During the first stage, the shear stress τ(t) sharply increases [see Fig. 5(a) between arrows a and b] with only a brief relaxation event (at0.85 GPa between 1 and 2 ns) resulting from the flattening of small surface obstacles. At about 9 ns, τ(t) reaches a maximum of 1.75 GPa due to asperity interlocking, which is accompanied by moderate grain refinement near the initial sliding interface. The formation of new grains and grain boundaries is detected by the steady increase in the non-bcc to bcc atom ratio R(t) in Fig. 5(a) between 2 and 9 ns. This grain refinement and the accompanying shear resistance enhancement is characteristic of a Hall-Petch-type mechanism.

Continued asperity interlocking from 4 to 9 ns [between Figs. 4(a) and 4(b)] leads to grain rotation and plastic deformation which in turn causes the counter bodies to cold weld [see Fig. 4(b)]. In the next stage of sliding (10 to 19 ns), the grains in the vicinity of the sliding zone gradually coarsen and merge, eventually forming a large grain that extends over the whole horizontal length of the simulation box [compare the top panels of Figs. 4(b) and 4(c)]. In a Hall-Petch fashion, this coarsening period is characterised by a marked decrease in τ(t) [see Fig. 5(a) between arrows b and c].

The sliding mechanism changes drastically between 19 and 38 ns, during which the sliding motion becomes confined within narrow shear zones spanning the entire horizontal distance of the system [see the bottom panels of Figs. 4(d) and 4(e)]. These NSBs are partly composed of twin boundaries [red zones indicated by the arrow in the middle panels of Fig. 4(d) and 4(e)], which propagate vertically within the coarsened grain. The evolution of this twinning phase is captured by the increase and decrease in R(t) displayed in

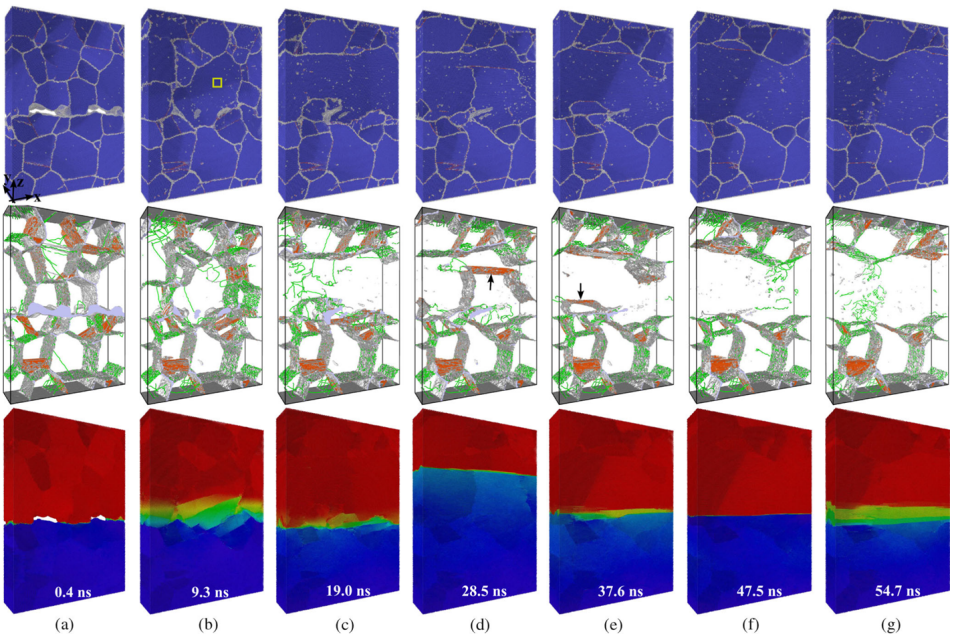

Figure 4. Snapshots of the evolution of sliding contact between two nanocrystalline iron tribo-partners. Each column presents the instantaneous state of the grain structure (top panel), the grain boundaries and dislocations (middle panel), and the corresponding sliding interface (bottom panel) at selected sliding times. The grain structure in the top row is exposed by performing a CNA[20] using a 3.46 cutoff radius (with blue, white, and red standing for bcc, non-bcc, and twin boundary atoms). The middle row shows the simultaneous state of the extracted dislocations[39,40] and twin boundaries (with green and gray lines representing dislocations with $1/2\langle 111\rangle$ and non-$1/2\langle 111\rangle$ Burgers vectors and with gray and red zones marking the location of voids and twin boundaries). In order to correlate the structural dynamics with the way the system distributes the sliding induced velocity gradient over the system, the strain rates are visualised in the bottom row by colouring the atoms according to their velocity along the sliding x-direction after every 0.2 ns on a scale from 0 m/s (blue) to 5 m/s (red). As sliding progresses, the counter bodies cold weld and establish a coarsened grain layer where plasticity concentrates and the sliding interface localises.

Fig. 5(a) between arrows c and e. Additionally, this interval contains the lowest values of the shear resistance τ(t) [see Fig. 5(a) between 22 $<$ t $<$30 ns] which is consistent with a low Peierls stress of twinning dislocations.

Interestingly, the first minimum in τ(t) at t $\sim$ 22 ns is accompanied by a realignment of the bcc $\langle 111\rangle$ close-packed direction within the coarse-grained layer along the direction of sliding. This is quantified in Fig. 5(b) by the change in the angle formed between the sliding x-direction and the $\langle 111\rangle$ lattice direction within the coarsening grain inside the region marked with a yellow rectangle in the top panel of Fig. 4(b). The starting misalignment of about 35^o at t $\sim$ 8 ns is progressively reduced until virtually a complete alignment with the direction of sliding is reached at $\sim$ 22 ns after which the orientation is maintained for the rest of the sliding time. These alignment changes can also be observed in the insets of Fig. 5(b) which show the atomic structure in the coarsened grain region for an observer looking along the direction of sliding.

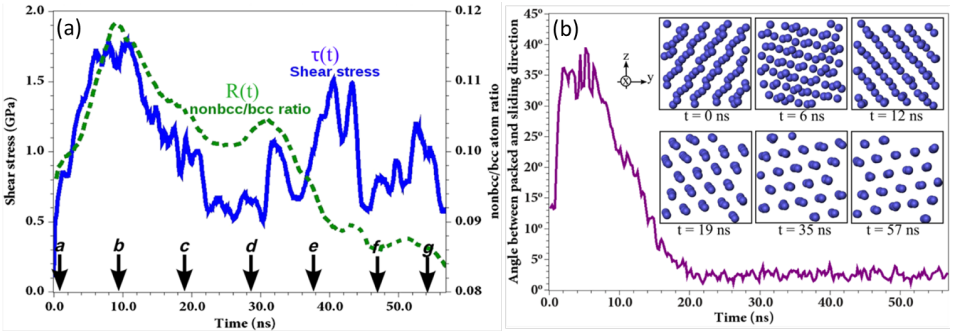

Figure 5. (a) Evolution of the shear stress [τ(t)] showing the materials resistance along the direction of sliding and the progression of the ratio of non-bcc to bcc atoms [R(t)] indicating the general reduction in the number of grains and grain boundary volume. The arrows recall the instances corresponding to the snapshots in Fig. 4. (b) Evolution of the bcc packed direction within the coarsened centre grain. The graph shows the angle between the bcc $\langle 111 \rangle$ packed direction and the sliding x-direction. The close-up insets show states of the crystal structure within the coarsened grain while looking in the direction of sliding. Clearly, the coarsened grain region strongly aligns its bcc packed direction along the direction of sliding.

4 Concluding Remarks

In conclusion, the large-scale MD simulations presented here demonstrate how computationally intensive atomistic simulations using high performance computing facilities can lead to fundamental understanding in tribology and machining processes. For instance our massive MD simulations for a hard asperity sliding on a metal surface shows that differently oriented slip systems between neighbouring surface grains along with lattice defects (i.e. GB) dictate the degree of material bulging towards the surface and the shape and size of the resulting surface folds. The chosen simulation conditions favour dislocation-mediated processes that are by no means restricted to nanoscale grains but are rather well documented for texture formation in conventional polycrystalline metals[41]. Therefore, plasticity-induced bulging around surface extending lattice defects (e.g., GBs) can be regarded as the elementary process underlying fold formation in polycrystalline metals, which represents an important mechanism for the generation of lamellar wear debris (as suggested by nano-wear experiments).

As shown by the large-scale spatial ($\sim$5.6 million atoms) and temporal (58 ns) atomistic simulations for metal on metal sliding contact, pure nanocrystalline metallic surfaces tend to undergo grain coarsening at the contact interface during extensive sliding plastic shear. Once the interface grains cold weld, they self-organise by coarsening through grain boundary migration and by simultaneously reorienting the lattice of the coarsening grains until the optimal plastic slip direction is aligned with the sliding direction. Subsequently, the relative sliding motion is accommodated through heavily localised NSBs and twin boundary planes located within the coarsened textured interface grains. This grain coarsening and realignment in conjunction with the reduction of frictional resistance exemplifies the tendency of tribologically driven systems to self-organise during a running-in phase in order to create more easily deformable material layers at the sliding interface[42,43].

Acknowledgements

We acknowledge funding support from the Deutsche Forschungsgemainschaft (DFG), the Robert Bosch GmbH, and the European Commission under Contract No. NMP.2010.2.5-1.263335 (MultiHy). Simulations were conducted on the supercomputer JUROPA and JUQUEEN at the Jülich Supercomputing Centre (JSC). Visualisation was mainly carried out with OVITO[39,40].

References

1. S. J. Plimpton, *Fast parallel algorithms for short-range molecular dynamics*, J. Comp. Phys. **117**, 1–19, 1995.
2. `http://www.fz-juelich.de`
3. F. P. Bowden and D. Tabor, *The Friction and Lubrication of Solids*, Clarendon Press, Oxford, 1950.
4. F. P. Bowden, A. J.W. Moore, and D. Tabor, *The ploughing and adhesion of sliding metals*, J. Appl. Phys **14**, 80, 1943.
5. K. L. Johnson, *Contact mechanics and the wear of metals*, Wear **190**, 162, 1995.
6. P. L. B. Oxley, *The Mechanics of Machining: An Analytical Approach to Assessing Machinability*, Halsted Press, New York, 1989.
7. P. A. Romero, G. Anciaux, A. Molinari, and J.-F. Molinari, *Friction at the toolchip interface during orthogonal nanometric machining*, Model. Simul. Mater. Sci. Eng **20**, 055007, 2012.
8. P. A. Romero, G. Anciaux, A. Molinari, and J.-F. Molinari, *Insights into the thermomechanics of orthogonal nanometric machining*, Comput. Mater. Sci. **72**, 116, 2013.
9. P. Berlet, M. Dienwiebel, and M. Scherge, *The effect of sample finishing on the tribology of metal/metal lubricated contacts*, Wear **268**, 1518, 2010.
10. P. Iglesias, M. D. Bermdez, W. Moscoso, and S. Chandrasekar, *Influence of processing parameters on wear resistance of nanostructured OFHC copper manufactured by large strain extrusion machining*, Wear **268**, 178, 2010.
11. Peter J. Blau, *On the nature of running-in*, Tribol. Int. **38**, 1007, 2005.
12. N. K. Sundaram, Y. Guo, and S. Chandrasekar, *Mesoscale folding, instability, and disruption of laminar flow in metal surfaces*, Phys. Rev. Lett. **109**, 106001, 2012.
13. A. Emge, S. Karthikeyan, and D. Rigney, Wea **267**, 562, 2009.
14. P. Stoyanov, P. A. Romero, T. T. Järvi, L. Pastewka, M. Scherge, P. Stemmer, A. Fischer, M. Dienwiebel, and M. Moseler, Tribol. Lett. **50**, 67, 2013.
15. A. Zhilyaev, S. Swaminathan, A. Pshenichnyuk, T. Langdon, and T. McNelley, J. Mater. Sci. **48**, 4626, 2013.
16. K. Zhang, J. R. Weertman, and J. A. Eastman, Appl. Phys. Lett. **87**, 061921, 2005.
17. M. Jin, A. Minor, E. Stach, and J. W. Morris Jr., Acta Mater. **52**, 5381, 2004.
18. X. Z. Liao, A. R. Kilmametov, R. Z. Valiev, H. Gao, X. Li, A. K. Mukherjee, J. F. Bingert, and Y. T. Zhu, Appl. Phys. Lett. **88**, 021909, 2006.
19. B. Boyce and H. A. Padilla II, Metall. Mater. Trans. A **42**, 1793, 2011.
20. J. D. Honeycutt, and H. C. Andersen, *Molecular dynamics study of melting and freezing of small Lennard-Jones clusters*, J. Phys. Chem. **91**, 4950, 1987.

21. P. A. Romero, T. T. Järvi, N. Beckmann, M. Mrovec, and M. Moseler, *Coarse graining and localized plasticity between sliding nanocrystalline metals*, Phys. Rev. Lett. **113**, 036101, 2014.
22. M. Chandross and E. A. Holm, *Measuring grain junction angles in discretized microstructures*, Metall. Mater. Trans. A **41**, 3018, 2010.
23. D. P. Field, L. T. Bradford, M. M. Nowell, and T. M. Lillo, *The role of annealing twins during recrystallization of Cu*, Acta Mater. **55**, 4233, 2007.
24. D. Farkas, E. Bringa, and A. Caro, *Annealing twins in nanocrystalline fcc metals: A molecular dynamics simulation*, Phys. Rev. B **75**, 184111, 2007.
25. Y. Mishin, M. J. Mehl, D. A. Papaconstantopoulos, A. F. Voter, and J. D. Kress, *Structural stability and lattice defects in copper: Ab initio, tight-binding, and embedded-atom calculations*, Phys. Rev. B **63**, 224106, 2001.
26. E. Bitzek, P. Koskinen, F. Gähler, M. Moseler, and P. Gumbsch, *Structural relaxation made simple*, Phys. Rev. Lett. **97**, 170201, 2006.
27. H. J. C. Berendsen, J. P. M. Postma, W. F. van Gunsteren, A. DiNola, and J. R. Haak, *Molecular dynamics with coupling to an external bath*, J. Chem. Phys. **81**, 3684, 1984.
28. E. A. Holm, and S. M. Foiles, *How grain growth stops: A mechanism for grain-growth stagnation in pure materials*, Science **328**, 1138, 2010.
29. R. D. Groot, and P. B. Warren, *Dissipative particle dynamics: Bridging the gap between atomistic and mesoscopic simulation*, J. Chem. Phys. **107**, 4423, 1997.
30. G. Simonelli, R. Pasianot, and E. Savino, Mater. Res. Soc. Symp. Proc. **291**, 567, 1993.
31. M. Müller, P. Erhart, and K. Albe, J. Phys. Condens. Matter **19**, 326220, 2007.
32. L. Pastewka, S. Moser, M. Moseler, B. Blug, S. Meier, T. Hollstein, and P. Gumbsch, Int. J. Mat. Res. **99**, 1136, 2008.
33. T. Soddemann, B. Dünweg, and K. Kremer, Phys. Rev. E **68**, 046702, 2003.
34. N. Beckmann, P. A. Romero, D. Linsler, M. Dienwiebel, U. Stolz, M. Moseler, P. Gumbsch, *Origins of Folding Instabilities on Polycrystalline Metal Surfaces*, Phys. Rev. Applied **2(6)**, 06400, 2014.
35. D. Farkas, A. Frseth, and H. van Swygenhoven, *Grain boundary migration during room temperature deformation of nanocrystalline Ni*, Scr. Mater. **55**, 695, 2006.
36. Y. Cheng, D. Weygand, and P. Gumbsch, *Simulation of small-angle tilt grain boundaries and their response to stress*, Comput. Mater. Sci. **45**, 783, 2009.
37. J. W. Cahn, Y. Mishin, and A. Suzuki, *Coupling grain boundary motion to shear deformation*, Acta Mater. **54**, 4953, 2006.
38. J. Schiotz, F. D. D. Tolla, and K. W. Jacobsen, Nature **London**, 391, 5611998.
39. A. Stukowski, Model. Simul. Mater. Sci. Eng. **18**, 015012, 2010.
40. A. Stukowski, V. V. Bulatov, and A. Arsenlis, Model. Simul. Mater. Sci. Eng. **20**, 085007, 2012.
41. D. Helm, A. Butz, D. Raabe, and P. Gumbsch, *Microstructure-based description of the deformation of metals: Theory and application*, JOM **63**, 26, 2011.
42. M. Godet, Wear **100**, 437, 1984.
43. Y. Berthier, M. Godet, and M. Brendle, Tribol. Trans. **32**, 490, 1989.